



Krijgsman, W., Rohling, E. J., Palcu, D., Raad, F., Amarathunga, U., Flecker, R. M., Florindo, F., Roberts, A., Sierro, F. J., & Aloisi, G. (2024). Causes and consequences of the Messinian salinity crisis. *Nature Reviews Earth and Environment*, 5(5), 335-350. Advance online publication. <https://doi.org/10.1038/s43017-024-00533-1>

Peer reviewed version

License (if available):
CC BY

Link to published version (if available):
[10.1038/s43017-024-00533-1](https://doi.org/10.1038/s43017-024-00533-1)

[Link to publication record in Explore Bristol Research](#)
PDF-document

This is the accepted author manuscript (AAM) of the article which has been made Open Access under the University of Bristol's Scholarly Works Policy. The final published version (Version of Record) can be found on the publisher's website. The copyright of any third-party content, such as images, remains with the copyright holder.

University of Bristol - Explore Bristol Research

General rights

This document is made available in accordance with publisher policies. Please cite only the published version using the reference above. Full terms of use are available:
<http://www.bristol.ac.uk/red/research-policy/pure/user-guides/ebr-terms/>

Causes and consequences of the Messinian salinity crisis

Wout Krijgsman^{1,†}, Eelco J. Rohling², Dan V. Palcu^{1,3}, Fadl Raad⁴, Udara Amarathunga⁵, Rachel Flecker⁶, Fabio Florindo⁷, Andrew P. Roberts⁵, Francisco J. Sierro⁸, and Giovanni Aloisi⁹

¹ Department of Earth Sciences, Utrecht University, Utrecht, The Netherlands.

² Ocean and Earth Science, University of Southampton, Southampton, UK

³ National Institute of Marine Geology and Geo-ecology, GeoEcoMar, Bucharest, Romania

⁴ Department of Hydrogeology, University of Corsica Pasquale Paoli, Corte, France.

⁵ Research School of Earth Sciences, Australian National University, Canberra, Australia.

⁶ BRIDGE, School of Geographical Sciences and Cabot Institute, University of Bristol, Bristol, UK.

⁷ Istituto Nazionale di Geofisica e Vulcanologia, Rome, Italy.

⁸ Department of Geology, University of Salamanca, Salamanca, Spain.

⁹ Institut de Physique du Globe de Paris (IPGP), Université Paris Cité, CNRS, Paris, France.

[†]e-mail: W.Krijgsman@uu.nl

Abstract

Salt giants are massive salt deposits (at least hundreds of m thick) that form during the evaporation of semi-enclosed seas. However, the drivers of salt giant formation and their feedbacks on global and regional environmental change remain debated. In this Review, we summarize the boundary conditions, causes and consequences of the Mediterranean Messinian salinity crisis (MSC; 5.97-5.33 Ma), and highlight the impacts of salt extraction and ion return on the Earth system. Salt giant formation is more complex than the simple evaporation of an enclosed sea. Instead, the tectonic setting of an evaporative basin largely determines the timing and mode of salt formation, with superimposed impacts of orbital-scale climate and sea-level fluctuations. These drivers triggered precipitation of carbonates, gypsum, halite, and even bittern salts in the Mediterranean, with well-defined orbital cyclicities in carbonate and gypsum phases. Removal of Ca^{2+} during salt deposition decouples the oceanic Ca^{2+} and HCO_3^- sinks, causing a CaCO_3 burial decrease and, consequently, increased ocean pH, lower atmospheric $p\text{CO}_2$, and global cooling. Salt giants, which reflect a ~7 to 10 % net evaporite-ion extraction from oceans that persists over million-year timescales, could therefore be an important climatic driver, but are currently not considered in long-term carbon cycle models. Future research should target more advanced hydrogeochemical models of water exchange with the open ocean to provide critical context for understanding interactions between salt giants and environmental change.

Website Summary:

Tectonic processes can lead to the formation of nearly enclosed seas and the deposition of extensive salt deposits. This Review explores the drivers and impacts of the Mediterranean Messinian salinity crisis, including previously under-considered impacts on the global carbon cycle.

Key points

1. Giant salt deposits (gypsum and halite) formed in the Mediterranean during the Messinian Salinity Crisis and their timing and mode depended on tectonic impacts on the evaporative basin.
2. Geodynamic and eustatic sea-level forcing are crucial for initiating and terminating salt giant formation with a subsidiary role for regional climate.
3. The main controls on evaporitic mineral precipitation are the freshwater deficit magnitude and the extent of water-exchange limitation between basin and ocean.
4. Evaluation of an updated sea-level record for the 6.4 to 5.0 Ma time interval demonstrates that sea level is a viable driver of the prominent MSC sedimentary cyclicality in addition to orbital freshwater budget variation.
5. The formation and dissolution of giant calcium sulphate (gypsum and anhydrite) deposits can have global consequences as an episodic driver of carbon cycle changes. Oceanic Ca^{2+} removal via CaSO_4 deposition decouples the oceanic Ca^{2+} and HCO_3^- sinks, causing a CaCO_3 burial decrease and, consequently, increased ocean pH, lower atmospheric $p\text{CO}_2$, and global cooling.
6. Most biogeochemical models assume that evaporite precipitation and weathering are balanced over timescales >100 kyr. However, salt giants can reflect a ~ 7 to 10 % net evaporite-ion extraction from ocean water that persist over million-year timescales, suggesting that current carbon cycle models could be missing an important long-term climatic driver.

[H1] Introduction

[Paragraph 1 – importance] The opening and closure of oceans and seas by plate tectonic processes is often marked by formation of marginal basins that have restricted water-exchange with the open ocean. Under negative hydrological budgets, where freshwater loss by evaporation exceeds the supply from rivers and rainfall, periods of limited exchange with the open ocean can lead to precipitation of enormous evaporite deposits in the incipient or dying basin, termed ‘salt giants’. A small-scale modern example of an evaporative basin is the Dead Sea, a deep hypersaline lake that is entirely disconnected from the ocean. Salt giants have formed episodically through Earth’s history, including the Palaeozoic (Australia, USA, Russia, NW Europe), Mesozoic (South Atlantic, Gulf of Mexico), and Cenozoic (Mediterranean, Red Sea, Central Europe) eras^{1,2}. Halite (NaCl) and gypsum or anhydrite (CaSO₄) extraction from seawater during salt giant formation can represent >5% of the total ocean dissolved salt content^{3,4}, which disrupts local ecosystems in evaporitic seas and modifies global ocean chemistry⁵.

[Paragraph 2 – MSC key features] The Mediterranean Messinian salinity crisis (MSC) is one of the youngest salt giants in Earth’s history, having formed between 5.97 and 5.33 Ma when the Mediterranean became land-locked in the Late Miocene. During the MSC, more than one million cubic km of salt was extracted from the global ocean and precipitated as hundreds of m-thick gypsum deposits and km-thick halite units in the Mediterranean basins. The marine Atlantic connection progressively closed and Mediterranean water level has been interpreted to drop 800-2000 m⁶⁻⁸. During the final MSC stage, also known as “Lago Mare”, the Mediterranean transformed into a megalake with highly fluctuating, hypersaline to brackish, conditions. The MSC was terminated by a massive flood from the Atlantic that reintroduced open marine conditions across the Miocene-Pliocene boundary in the Mediterranean⁹⁻¹¹.

[Paragraph 3 – motivation/recent developments] Seismic profiles across deep basinal sequences and outcrops along tectonically uplifted marginal basins provide a picture of the spatial distribution of Mediterranean evaporite units and their stratigraphy (Fig. 1)¹²⁻¹⁶. The Late Miocene land-locked Mediterranean configuration amplified its responses to regional and global climate fluctuations, and caused distinct cycles in pre- and post-MSC deposits, facilitating construction of a detailed chronostratigraphic framework, tuned with

precessional resolution (~20 kyr) to astronomical insolation curves^{17–19}. This astrochronology has resulted in a stratigraphic consensus scenario for the Mediterranean salt giant¹⁵ that provides a foundation for high-resolution geochemical evaporite fingerprinting^{20,21} and for observational and modelling studies of the underlying forcing mechanisms^{22,23}. These advances indicate that salt giants do not form in basins that simply isolate and desiccate; rather, complex sub-basin settings have a crucial role in determining the timing and mode of salt formation^{24,25}, with contributions from various forcing mechanisms such as tectonics, sea-level change, and hydrological connectivity with the ocean²⁶.

[Paragraph 4 – In this Review, we..] In this Review, we discuss the latest developments in MSC research, in terms of salt formation, hydrological conditions and drivers of basin desiccation. We build on previous detailed overviews of MSC stratigraphy^{15,27}, Mediterranean evaporite distribution patterns^{4,16}, and Atlantic-Mediterranean connectivity^{26,28}, and expand on the drivers and feedbacks of the MSC that are applicable to other salt giants more generally. In particular, we reflect on the regional and global environmental consequences of salt giant formation, rapid ion return during basin reconnection, and slow ion return during weathering over geological timescales, including impacts on the global carbon cycle.

[H1] The Mediterranean salt giant

Tectonic processes can lead to near-isolation of continental seas and deposition of extensive salt deposits. The onset of MSC evaporite deposition and establishment of earliest Pliocene marine conditions provide insights into both restriction and re-opening of such a marginal sea. The Mediterranean salt giant formed in a convergent plate tectonic setting with the African plate moving northward with respect to Europe and Iberia. This convergence is not complete, so it is possible that the Messinian evaporites will, in time, represent merely the initial phase of salt giant formation associated with ongoing Mediterranean basin closure.

[H2] Geological setting of the MSC

Salt giant formation requires the presence of a sill that restricts an evaporative basin from the open ocean. These sills generally form when continents collide or break apart by plate tectonic processes and provide the necessary raised lip across which exchange becomes restricted and allows development of water bodies with different

chemical and physical properties. The strait at Gibraltar that connects the Mediterranean with the Atlantic is presently 284 m deep at the Camarinal sill and 14.3 km wide at the Tarifa narrows²⁹. Palaeogeographic reconstructions of the Gibraltar region indicate that the early Messinian Atlantic-Mediterranean connection was a foreland-basin system with multiple gateways through southern Iberia and northern Morocco^{26,28}. These Betic and Rifian corridors, respectively, closed progressively in pre-MSB times, and marine connectivity evolved toward a single proto-Gibraltar strait gateway for the MSB^{28,30}. Mediterranean-Atlantic connectivity could also have been partially controlled by an emergent volcanic chain on the eastern Alborán margin that formed a partial land-bridge between northern Morocco and southeastern Spain³¹. Water flux modelling indicates that exchange patterns with the Atlantic depended on relative sill depths³². Crucially, two-way flow exists in both corridors when the shallowest corridor is more than half as deep as the deepest corridor, whereas one-way flow exists in both corridors when the shallowest corridor is less than half as deep as the deepest corridor³². Uplift of the Rifian corridor at ~ 7 Ma³⁰ could, therefore, have altered exchange patterns in the Gibraltar strait from mainly Atlantic inflow to two-way flow, consistent with simultaneous Alborán Basin benthic faunal changes³³ and deep Mediterranean records in which the first signs of restricted conditions and increased water mass stratification occurred at ~ 7 Ma³⁴.

[H2] MSB stratigraphy

Mediterranean Messinian evaporites were first reported in 1867³⁵ and were later described by field geologists who documented ~ 100 -m-thick gypsum units between marine sequences in several Italian basins^{36,37}. In the 1970s, the widespread presence of evaporite units across the Mediterranean was confirmed by Deep Sea Drilling Project (DSDP) Leg 13^{3,38,39}, although coring only reached the uppermost MSB successions.

The depositional and stratigraphic architecture of Messinian evaporites varies across the Mediterranean, and depend mainly on tectonic settings and water depths. Four main settings are recognized (Fig. 2). First, marginal zones with mainly erosional features that have commonly been related to multiple drawdown events^{6,16} in which subaqueous erosion by dense cascading waters might also have had a role⁴⁰. Second, shallow, silled basins (Adriatic region, SE Spain basins) containing the most complete marine gypsum successions⁴¹, overlain in places by erosional surfaces and/or younger lacustrine and continental deposits with intervals characterized by

brackish Lago Mare fauna^{24,42-44}. Third, intermediate-depth basins (Sicily, Cyprus, Balearic Promontory), which can be complicated by substantial tectonic deformation during and since the MSC^{45,46}. Basal MSC units in these intermediate settings comprise marine gypsum⁴⁷ or anoxic shales devoid of evaporites^{48,49}. Where marine gypsum is observed, the evaporites might not be preserved *in situ* because they are commonly found as a range of reworked deposits from gypsarenites to gypsum olistostromes^{15,50}. The final, fourth setting includes deep central basins that are found in the western (Liguro-Provençal, Algerian) and eastern (Ionian, Levant) Mediterranean, separated by the Strait of Sicily, which have strikingly different depositional architecture on seismic reflection profiles^{12,16}.

Deep central western Mediterranean basins typically contain a seismic “trilogy” with a Lower Unit (mass-transport deposits), Mobile Unit (halite), and an Upper Unit (gypsum-clastic alternations)¹². However, no direct lithological data are available for the deep central western salt giant where only the topmost MSC has been sampled, which generally contains gypsum with brackish water fauna⁵¹. The easternmost deep Mediterranean (Levant Basin) contains a >1-km-thick evaporitic succession with six seismic sub-units^{52,53}, four transparent units composed of halite and two units composed of claystones^{54,55}. Cuttings from industrial drill holes suggest that evaporite deposition started with only a few metres of anhydrite^{52,56}, followed by the halite-dominated succession, which terminated after a truncation surface with a ~100 m thick “Unit 7” composed of shales, sands, and anhydrite¹⁴. This top unit of the MSC in the deep Levant Basin is interpreted as having been deposited above the Intra Messinian Truncation Surface (IMTS), a dissolution surface related to substantial dilution and stratification of the eastern Mediterranean water column¹⁴.

Detailed stratigraphic studies from both onshore sequences and offshore seismic data indicate that the Mediterranean contains several different evaporite successions (Fig. 1, 2)¹⁵. There are at least four main evaporitic deposit types observed in MSC successions now exposed on land. Evaporitic carbonates known as the Calcare di Base (Sicily)^{57,58} and the Terminal Carbonate Complex (SE Spain)^{59,60} formed at the Messinian basin margins. Predominantly marine gypsum known as the Primary Lower Gypsum unit (PLG: Spain, Italy)^{21,41} mainly precipitated in depocentres of shallow silled basins. Downslope reworking of PLG by tectonic activity and gravitational sliding is a common feature in intermediate-depth basins (Sicily, Balearic

Promontory, Cyprus)^{46,61}. Thick gypsum-mudstone alternations and the absence of desiccation features indicate that Mediterranean-Atlantic connectivity persisted with two-way flow. Halite is only present in intermediate and deep central basins (Sicily, Liguro-Provençal, Levant)⁶². Marine inflow is still required to accommodate km-thick halite successions, but outflow was likely blocked. The youngest MSC evaporites are gypsum with continental geochemical signatures of the so-called Upper Gypsum unit (UG: Sicily, Cyprus)^{24,63}. This gypsum unit requires additional fresh-water influx from the Paratethys and alternates with clastics that contain brackish Lago Mare fauna²⁴. Also, volumetrically minor K-Mg-salts (bittern salts) are sometimes associated with halite. Except for the halite in the western Mediterranean, all of these evaporites are interbedded with detrital clastics and/or hemipelagic sediments. The transition from non-marine Messinian to deep marine Zanclean deposits marks the end of the MSC, and is often conformable without evidence of major erosion^{10,64}.

[H2] Astronomical cycles in Mediterranean evaporites

Miocene and Pliocene Mediterranean sedimentary successions are marked by precession-paced sapropel-marl cycles with characteristic patterns that can be correlated across the Mediterranean and to astronomical curves (Fig. 3)^{17,18,65}. The sapropels record humid conditions at precession minima and insolation maxima and the marls reflect arid conditions at precession maxima and insolation minima. Cyclostratigraphic correlation and astronomical tuning of pre- and post-MSC sedimentary successions provide accurate ages for both the onset of PLG precipitation (5.97 Ma)⁶⁶, with evaporitic limestones in some intermediate and marginal basins forming slightly earlier (6.08-6.03 Ma)^{13,67,68}, and the marine sediments that immediately overlie the MSC successions throughout the Mediterranean (5.33 Ma)⁶⁹. This astronomical tuning constrains the MSC duration to 640 kyr. Dating within the MSC interval itself is more uncertain because of a lack of high-resolution independent age control points; magnetostratigraphic constraints are lacking as the entire MSC occurred within a single reversed magnetic polarity subchron^{18,70} (Fig. 3), biostratigraphic markers are absent because of the extreme environmental conditions, and datable volcanic ash layers are scarce^{15,43}.

During the PLG phase, marine carbonate-marl and gypsum-marl cycles accumulated subaqueously in both shallow and intermediate basins (Fig. 3)⁴¹, which precludes a major Mediterranean sea-level fall at the onset of the MSC⁷¹. Moreover, marine strontium isotope data are broadly consistent with a high Mediterranean water

level that permitted restricted two-way Atlantic-Mediterranean exchange^{21,72}. Assuming that cyclic gypsum-marl alternations followed the same regional precessional climate forcing as pre- and post-MSC Mediterranean sediments, correlation of 16-17 documented sedimentary cycles in the PLG to astronomical curves suggest that PLG deposition ended at <5.6 Ma (Fig. 3)^{41,73}. However, numerical modelling of water and salt balances indicates that the gypsum-marl cycles could have resulted either from precession-driven ~20% hydrological budget changes and/or oscillating gateway restriction caused by sea-level fluctuations of ~10 m competing with tectonic uplift and marine gateway erosion^{74,75}.

Deep Mediterranean halite units lack absolute age control. In the western Mediterranean, halite is thought to have succeeded PLG deposition and is correlated tentatively with the TG12-14 glacial interval (5.59-5.55 Ma) in oxygen isotope ($\delta^{18}\text{O}$) records^{27,76} (Figs. 3, 4). The timing of initial eastern Mediterranean halite deposition is contested, with suggested ages ranging from 5.97 Ma, equivalent to the PLG onset in marginal basins⁷⁷, to 5.59 Ma, at the end of the PLG⁷⁸. There is a third possibility, that halite deposition partly coincided with the start of glacial stage TG22 at ~5.8 Ma, as demonstrated by comparing global sea level with MSC sill-depth scenarios (Fig. 4). Halite is thought to have been deposited when Atlantic-Mediterranean exchange was more restricted than during the PLG phase⁷⁹ (see also *Supplementary Note*). In geochemical models, a severely restricted scenario with no Mediterranean outflow (that is, with Mediterranean sea level close to, or below, sill depth) could support deposition within 80 kyr of the deep-basin halite body observed in seismic profiles⁷⁹. In this scenario, evaporated freshwater is replaced continuously by Atlantic inflow, which generates the necessary ion fluxes for halite deposition. The evaporite mineral paragenesis resulting from this constant marine supply with no ion loss via Mediterranean outflow is distinctly different from that generated by evaporation of a fixed seawater volume. Instead of sequential evaporite phases precipitating as brine concentration increases, mineral precipitation fields overlap substantially, with carbonate, gypsum, and halite precipitation potentially coexisting up to bittern salt formation⁸⁰.

The final Mediterranean salt giant phase is the most enigmatic, with alternating UG beds and brackish Lago Mare deposits that contain biota of Paratethyan (former Black Sea-Caspian Sea system) affinity⁴³. In intermediate basins (Sicily, Cyprus), 6-7 gypsum-brackish marl alternations are observed^{27,81}. Strontium

isotope ratios from both gypsum crystals in the UG and ostracods from Lago Mare marl horizons suggest a dominantly freshwater system with only minor (~20%) Atlantic contribution^{24,63}. Assuming that UG cycles were precession-driven, downward tuning from the lowermost Zanclean suggests that this final MSC phase started at 5.52 Ma²⁴. In shallow silled basins, time-equivalent continental and lacustrine sediments contain influxes of high-diversity Paratethyan ostracods, but no gypsum^{42,82}.

[H1] Salt giant forcing mechanisms

Marine gateways have a critical role in the exchange of water, heat, salt, and nutrients between oceans and seas. During the MSC, water exchange with the open marine Atlantic Ocean and the brackish Paratethys Sea were influenced by a complex combination of geodynamic (tectonic movements in gateway regions), glacio-eustatic (global sea level fluctuations), and palaeoclimatic (hydrological budget changes) processes that all had a role in Messinian salt giant formation. Tectonic uplift and sea level lowering can have similar effects on water exchange through gateways and are difficult to unravel. Here, we present and evaluate current understanding of the geodynamic, ice-volume and sea-level forcings on the MSC and then revisit the role of superimposed regional palaeoclimatic forcing.

[H2] Geodynamic forcing

The main geodynamic processes in the Gibraltar orogenic system involve African-Iberian plate convergence⁸³, slab tearing under the eastern Betic Cordillera⁸⁴, and mantle resistance against Gibraltar slab drag⁸⁵. Mantle tomography and other seismological investigations provide a clear present-day 3D image of Gibraltar slab geometry and lateral continuity with surface plates, and where it is detached and might have delaminated from continental lithospheric mantle (Fig. 5)^{84,86}. Early to Late Miocene westward slab roll-back resulted in thrusting of the Alborán domain over the African and Iberian margins. Indentation of the Rif Mountains by slab dragging together with slab detachment beneath the Betic Cordillera (Fig. 5a, b) can explain gateway opening, closure, and re-opening⁸⁷. During the late Tortonian (between 8 and 7 Ma), the Betic gateways were uplifted by isostatic rebound related to gradual slab tearing below Spain. Slab dragging initiated thick-skinned tectonics in Morocco that also closed the Rifian Corridor⁸⁸.

During the MSC, sills within the Mediterranean basin also had important roles. In shallow silled basins where PLG developed, geochemical evidence indicates that climate oscillations⁸⁹ modified conditions within the basins resulting in localised density contrasts across the sills, even before the MSC⁹⁰. The Sicily sill, which separates the western and eastern Mediterranean basins, had a crucial role in water and salt transport across the Mediterranean before, during, and after the MSC^{11,91,92}, and likely generated the different MSC stratigraphies in the deep central basins. Other important sills were the tectonically active Gargano promontory (Italy)⁹³ and Cyclades region (Greece)⁹⁴ that separate, respectively, the Adriatic and North Aegean basins from the open eastern Mediterranean (Fig. 1). These restricted basins persisted as two evaporite-free largely isolated megalake systems during the halite and UG phases, probably influenced by extensive European river runoff (Fig. 1)^{82,94}.

In the eastern Mediterranean, the marine Neo-Tethys connection to the Indian Ocean had already closed in mid-Burdigalian times (~19-17 Ma), driven by Africa-Arabia-Eurasia collision^{95,96}, which created the first land bridge for mammal migration into and out of Africa. Consequently, this gateway probably played no role in Messinian salt giant evolution. Instead, the most important eastern connection during the MSC was with the Paratethys domain (Fig. 1). The present-day connection has sills 55 m deep and 1.2 km wide at the Dardanelles near Çanakkale, and 36 m deep and 698 m wide at the Bosphorus near Istanbul⁹⁷ (Fig. 1a). Messinian palaeogeographic evolution of the Mediterranean-Paratethys gateway is poorly understood, but it affected hydrological, palaeoecological, and palaeoenvironmental conditions in both domains⁹⁴. Palaeontological data indicative of marine faunal exchange^{98,99} and strontium isotope data²³ suggest that Mediterranean-Paratethys connectivity was established at 6.1 Ma^{100,101}, before the onset of evaporite precipitation. Gateway geodynamics between the Mediterranean and Paratethys were then, as now, dominated by active westward growth and propagation of the North Anatolian Fault Zone, North Aegean extensional tectonics, and Cyclades domain uplift and exhumation¹⁰². These tectonic processes, combined with substantial lake-level fluctuations, resulted in episodic Mediterranean-Paratethys and Black Sea connection and disconnection ever since^{103,104}.

[H2] Glacio-eustatic forcing

To date, sea-level forcing of the MSC has been dismissed in most studies based on the assumption that its variations were obliquity controlled (~40 kyr); using this period for sedimentary cyclicity would result in an

MSC duration that is too long to match independent age constraints. However, an updated global $\delta^{18}\text{O}$ synthesis indicates that the periodicity of ice-volume and deep-sea temperature fluctuations across the Late Miocene was controlled by precession, similar to Mediterranean climate cycles (Fig. 4)¹⁰⁵. To assess whether sea level was an important forcing mechanism for Mediterranean isolation from, and/or reconnection to, the Atlantic Ocean¹⁰⁶, we examine an updated sea-level record for the 6.4 to 5.0 Ma time interval relative to the present level (0 m; Fig. 4). By applying established box-model approaches to evaluate the evaporite implications of gateway restriction⁷⁴ (see *Supplementary Note*), this updated sea-level record indicates that sill depths >41 m favour basinal hemipelagic carbonate (marl) deposition. Evaporative carbonate deposition is favoured when the strait depth ranges between 22 and 41 m, gypsum deposition occurs between 13 and 22 m, and halite deposition occurs at depths <13 m. Friction would reduce exchange through the strait, so these threshold water depths are minimum estimates.

The updated high-resolution record of global mean sea-level variations¹⁰⁷ indicates that sea level alone cannot account for either the MSC onset, or rapid reestablishment of normal open marine conditions at the beginning of the Pliocene. Tectonic strait restriction is needed to trigger the transition from open marine hemipelagites to evaporative carbonates (6.08-6.03 Ma) followed by gypsum precipitation from 5.97 Ma (Fig. 4), while the MSC termination requires catastrophic, tectonic, strait opening to depths more than ~40 m below the lowest sea level of that time^{9,11}. However, some stratigraphic features within the MSC are consistent with Late Miocene sea level fluctuations. For example, with a shallow Mediterranean-Atlantic sill depth of 13-22 m (with the uplifted sill ~18 m below present-day sea level), sea-level fluctuations could explain the 16 gypsum cycles (magenta arrows in Fig. 4b) deposited during the PLG phase. In this scenario, sea-level influence on the gypsum cycles could have been irregular, potentially accounting for at least some observed variability in their thickness and spacing. These lithological threshold depth calculations ignore Paratethys inputs and precession-scale Mediterranean hydrologic budget fluctuations, which are likely to have varied; threshold depths will be somewhat smaller under more humid conditions and somewhat greater under more arid conditions (see⁷² for sensitivity analysis). Changes in Paratethys inputs and Mediterranean hydrology might explain the absence of halite between 5.8 and 5.7 Ma, when it should have been triggered by two marked sea-level falls (Fig. 4b). The

onset of well-documented halite precipitation (at ~5.6 Ma) requires further tectonic strait restriction (red shading in Fig. 4b). Maximum gateway restriction occurred at 5.55 Ma when global sea level was lowest, consistent with an episode of Mediterranean sea level fall. The end of halite deposition could have been terminated by the sea-level rise at ~5.53 Ma if the sill was below 6 m above present sea level.

For the UG phase (green shading in Fig. 4b), a (virtually) closed Atlantic connection with the basin in an essentially drawn-down state is required to obtain regional brackish to brine-water “lakes”, non-marine evaporite deposition, and continental-dominated Sr-isotope ratios^{11,24,25}. This high-resolution sea-level record is consistent with (potentially seven) partial reconnection events (green arrows in Fig. 4b) associated with minor Atlantic inflow that might correspond to the seven gypsum cycles observed in the UG^{24,81}.

[H2] Palaeoclimate forcing

Salt giant formation requires an excess of evaporation over precipitation and runoff into the basin. These factors are difficult to quantify from geological records and reconstructions. For example, palaeo-runoff requires robust knowledge of the palaeogeographic evolution of the complete catchment area of an evaporite basin, including its orography and palaeo-channels. However, global climate models can provide some constraints^{65,108,109}. We here evaluate climatic variations over the Mediterranean basin and its catchment area, including the Paratethys and the north African monsoon region immediately before, during, and after the MSC.

Several records indicate that the Mediterranean salt giant formed during a period of global cooling between 7.2 and 5.5 Ma^{110–112}, which is likely to have been triggered by a global atmospheric $p\text{CO}_2$ decline to a minimum between 6.5 and 5.8 Ma¹¹³. The Late Miocene $p\text{CO}_2$ decrease has been linked to a ~1 ‰ global benthic foraminiferal $\delta^{13}\text{C}$ drop known as the Late Miocene Carbon Isotope Shift (LMCIS; Fig. 3) between 7.6 and 6.6 Ma^{33,114}. This drop is amplified in the Mediterranean, probably because of progressive gateway restriction in the Gibraltar region since ~7.1 Ma¹¹⁵. The absence of a humidity decrease from the pre-evaporitic marls to the base of the PLG gypsum^{116,117} implies that MSC salt giant formation was not likely triggered by Mediterranean climate change. As atmospheric $p\text{CO}_2$ began to rise after 5.5 Ma, warming occurred¹¹³. This warming trend started at the transition between isotope stages TG12 and TG11, coincident with the end of halite deposition

and the onset of Mediterranean UG formation (Figs. 3, 4). Ensuing long-term global warming was associated with long-term global sea level rise^{106,107,118}.

Lack of foraminifera hinders Mediterranean palaeoclimate reconstructions through the MSC, although Messinian palynological¹¹⁹ and organic biomarker records^{120–123} indicate that Mediterranean climate was warm and dry before, during, and after the MSC. Along the northern Mediterranean margin, climate was warm and humid, similar to present-day conditions, with important river runoff from the Alps (Rhône and Po)¹²⁴. Lack of marked vegetation changes during the different evaporite phases suggests that Mediterranean climate did not force the MSC and that the MSC, in turn, did not have a substantial impact on Mediterranean climate¹¹⁹.

The classic marl-sapropel alternations of pre-evaporitic MSC successions indicate conspicuous precession-paced climate oscillations (Fig. 3)^{17,18,67}, in which sapropels mark relatively wet conditions during precession minima (insolation maxima), when enhanced freshwater runoff increased Mediterranean water column stratification¹²⁵. Whatever the role of eustatic sea-level variation, precessional forcing is assumed to have continued in the PLG deposits, with gypsum beds corresponding to relatively dry climates during precession maxima (insolation minima)^{41,73}. Organic geochemical data from PLG cycles in northern Italy confirm this, revealing climatic oscillations²¹ with gypsum deposition during relatively dry periods with reduced river runoff^{116,117}.

Most MSC scenarios envisage a maximum Mediterranean lowstand during or after halite deposition, with draw-down estimates of -600 to -2000 m^{6–8}, indicating a strong regional circum-Mediterranean negative hydrological balance. Mediterranean water level during the UG is still contested⁴³. The presence of recurrent, high-diversity, shallow-water, brackish ostracod assemblages in most shallow, silled Mediterranean basins indicates considerable net freshwater influxes. Palaeoclimate models suggest that Mediterranean-wide Lago Mare conditions cannot be explained by Paratethys inflow alone, and that additional water sources are required^{109,126}. Specifically, runoff from high-amplitude African monsoon maxima has been considered^{127–130}. Alternatively, Atlantic input to the basin might have contributed during glacio-eustatic relative sea level highstands (Fig. 4), although fully marine conditions were not established until the Zanclean⁶⁹.

Given Mediterranean regional hydroclimate constancy through the MSC, periods of strong evaporative water-level drawdown must reflect low net precipitation over remote parts of the Mediterranean freshwater catchment (Paratethys and/or monsoonal Africa). Conversely, major freshwater influx periods must reflect high net precipitation over far reaches of its catchment. The Paratethys is a likely source of considerable Messinian freshwater variations because connection between the two basins^{98,131} would have greatly extended the Mediterranean freshwater catchment area relative to today. Specifically, the Messinian Paratethys unified the Dacian, Black Sea, and Caspian Sea basins^{100,131}, so that all major Eurasian rivers (Danube, Dnjepr, Don, Volga, Syr-Darya, Amu-Darya) drained into the Mediterranean¹³². In the Tortonian, hydrological variations associated with eccentricity-driven northward (southward) mid-latitude westerly displacement over the Paratethys could have already caused decreased (increased) Paratethys overflow and runoff into the Mediterranean¹³³. Assuming that similar climate variability continued through the Messinian and that it also had a precession-timed component, the MSC net freshwater budget could have been affected substantially by Paratethys outflow^{108,126}.

African monsoon intensity tracked the northern summer insolation amplitude (hence the eccentricity-modulated amplitude of the precession cycle) throughout much of the Neogene^{127,128}, including the MSC^{129,130}. During insolation maxima (precession minima), monsoon-driven humidity expanded over north Africa^{127,128,134,135}. Large north African lakes, such as mega-lake Chad^{108,109}, might then have drained via the ancient Eosahabi river into the Mediterranean¹³⁶⁻¹³⁸. Although lake Chad lies well south of the modern central Saharan watershed, there is good evidence in younger geological periods of direct discharge via seasonal river floods and wadis^{139,140}. The absence of high-amplitude insolation maxima between 5.73 and 5.53 Ma suggests an extended interval of relatively weak African monsoons, whereas several high-amplitude insolation maxima during the UG phase suggest potential high-amplitude African monsoon maxima, with enhanced monsoon runoff into the Mediterranean basin (Fig. 3).

Overall, it appears that the long-term evolution from pre-evaporitic marls to gypsum and salt deposition was not driven predominantly by Mediterranean climate change, and that relative sea level drops interacting with tectonic changes at gateways and their impact on ocean water exchange likely were the main mechanisms

leading to progressive salt concentration. This long-term trend was punctuated by both precession-based cycles in sea-level and Mediterranean (including Paratethys and African monsoon) hydrology. The influence of these astronomically driven variations was amplified progressively as Mediterranean restriction increased.

[H1] Global relevance of the MSC

The MSC provides an illustration that salt giant formation is much more complex than simply evaporating a sea water volume following its oceanic disconnection. The Messinian salt giant transitioned through three restriction phases from the open ocean (Fig. 1, 2). First, restricted two-way exchange with maintained sea-level connection between the Mediterranean and Atlantic resulted in gypsum precipitation with marine geochemical signatures (PLG phase). Second, severely restricted oceanic inflow, sufficient to maintain evaporite ion flux while Mediterranean sea-level fell, drove halite deposition. Third, extremely limited, intermittent oceanic inflow led to continental-dominated, non-marine evaporite deposition alternating with brackish water conditions (UG phase). The sequence was terminated by abrupt reconnection and progressive restoration of normal marine conditions throughout the basin, re-establishing two-way Mediterranean-Atlantic exchange in the early Pliocene^{11,24}. Return flux of MSC residual brine ions into the open ocean occurred over ~30,000 years¹¹ (Fig. 6) and its impacts on open ocean circulation and climate have yet to be investigated.

Throughout all Mediterranean salt giant evaporitic phases, precession-timed runoff and/or global sea-level variations interacted to drive sedimentary environmental cyclicity due to greater or weaker freshwater admixtures and/or greater or weaker oceanic inflows to the basin, which overprinted marine connectivity changes due to tectonic gateway geometry changes. Model-based sensitivity tests indicate that even subtle freshwater budget and/or sea-level fluctuations would have sufficed to switch between gypsum and marl deposition⁷⁴. Precession-timed arid-to-humid and precession-timed sea-level cycles both occurred at amplitudes relevant to the sedimentary regime, but the precise phase relationship between their impacts remains elusive; these processes could have partially amplified or cancelled each other. More advanced hydro-geochemical models that integrate both forcing mechanisms will be required to fully understand gypsum formation under restricted marine conditions. Hydro-geochemical modelling of salt giants can also provide

useful information about the link between seawater-exchange restriction at the gateway sill and salinity evolution of the evaporite basin^{72,79,92}. These models track salinity as a single variable, or at most divide salinity into three contributions: gypsum (Ca and SO₄), halite (Na and Cl), and other salts (K, Mg, HCO₃⁻). This simplification, which facilitates numerical model solution, comes at the expense of a more correct thermodynamic description of the brine and its evolution during salt giant formation.

The exact drawdown amount remains a key unknown regarding halite and non-marine gypsum precipitation, when the evaporite basin was semi-isolated from the ocean. Maximum lowstands based on seismic interpretations combined with numerical modelling differ between -600 and -2000 m, assuming that all observed Messinian erosional surfaces formed subaerially. At times of severely restricted or negligible Atlantic inflow, Mediterranean evaporites are expected to contain a mineralogical imprint of continental runoff. The low Ca²⁺:Cl⁻ and SO₄²⁻:Cl⁻ in continental runoff enables gypsum precipitation at much lower salinities than when forming from evaporating seawater^{23,141}. Future hydro-geochemical models that integrate a sound thermodynamic description of high-salinity brines⁸⁰ will be able to test the hypothesis that increased relative importance of riverine inputs produces a substantial mineralogical assemblage change in a salt giant. Such models can also evaluate if a large (> 1.5 km) drawdown is required to attain brine saturation with respect to the highly soluble mineral bischofite, which is known to have precipitated during the MSC based on pore water geochemical tracers measured from the *Discovery*, *Hephaestus*, and *Kryos* deep-sea hypersaline brines on the Mediterranean Ridge¹⁴²⁻¹⁴⁴.

Almost all salt giant-related research to date has focused on their nature and causes^{15,145} with little consideration of their potential to drive wider environmental change^{146,147}, which is partly because of an assumption that impacts outside the salt basin will be synchronous with evaporite formation. Some MSC research has challenged that assumption^{24,148} and in doing so, has initiated new research into the chemical and physical consequences of the MSC and salt giants more generally for regional and global climate.

While the impact of evaporite formation and subsequent weathering on ocean chemistry has been known for some time¹⁴⁷, their potential to drive rapid carbon cycle changes and associated climate change remains enigmatic¹⁴⁶. Modelling of evaporite weathering and deposition suggests that despite the much larger halite

volume that is typically preserved in salt giants, it is the formation and dissolution of giant calcium sulphate (gypsum or anhydrite) deposits that can have global consequences as an episodic driver of carbon cycle changes¹⁴⁶. These global consequences could occur because oceanic Ca^{2+} removal via CaSO_4 deposition decouples the oceanic Ca^{2+} and HCO_3^- sinks, causing a CaCO_3 burial decrease and, consequently, increased ocean pH, lower atmospheric $p\text{CO}_2$, and global cooling. Similarly, the return of Ca^{2+} ions to the ocean from weathered gypsum can drive warming¹⁴⁶.

Most biogeochemical models have ignored evaporite-driven perturbations to seawater chemistry^{149,150}, assuming that over timescales >100 kyr, evaporite precipitation and weathering are balanced. Formation of km-thick MSC evaporites, and their preservation over the subsequent ~ 5 million years of Earth history, reflects a ~ 7 to 10 % net evaporite-ion extraction from ocean water over this period^{4,38}. Bearing in mind that the MSC is by no means the largest of the salt giants¹⁴⁷, this demonstrates that the evaporite precipitation-weathering balance assumption can only be true on multi-million year timescales at best, and suggests that current carbon cycle models could be missing an important intermediate timescale climatic driver¹⁴⁶.

Initial sensitivity experiments that explored the impact of gypsum precipitation and weathering on the carbon cycle recognised that precipitation and preservation of any gypsum represents a net reduction in oceanic $[\text{Ca}^{2+}]$ and expressed this as a constant Ca^{2+} forcing¹⁴⁶ for the duration of salt giant formation. However, in detail the Ca^{2+} ion flux associated with a salt giant is not constant, but far more complex, reflecting cyclic evaporite formation and the evolving connectivity history of the salt-bearing basin. For the MSC, this means that during the PLG, when gypsum-marl alternations formed under conditions of two-way Atlantic-Mediterranean exchange²⁶, Ca^{2+} ion loss from the global ocean occurred episodically, reflecting each precipitation event²⁴. It is also likely that return flux to the global ocean occurred as the newly formed gypsum layers partially dissolved²⁴. This return flux cannot have occurred during the later MSC stages, when there was no Mediterranean outflow²⁶. Any ions liberated by exposure and weathering of evaporites during periods of lowered Mediterranean sea level would have remained trapped within the basin at least until early Pliocene reestablishment of two-way exchange and flushing of residual brines which took $\sim 30,000$ years (Fig. 6)¹¹. New

model simulations that incorporate realistic Ca^{2+} ion flux records are, therefore, required to evaluate the magnitude of any evaporite-driven climate perturbation.

Reconstructing the magnitude and timing of evaporite ion fluxes is challenging. The salt volume preserved today is not a robust measure of the total evaporite ions extracted, but rather represents a minimum value for what was originally precipitated. Additional evaporites might have been precipitated and dissolved either before burial or during later exposure by orogenic processes⁵. Evaporite minerals also precipitate and dissolve three orders of magnitude more rapidly than other sediments¹⁵¹. Consequently, their impact on the carbon cycle can be an order of magnitude quicker than the carbonate-silicate weathering feedback¹⁴⁶. Through burial, evaporites can also be stored in rock successions for long periods outside the ocean-climate system²⁸. As a result, evaporite-mediated ion extraction from, and return to, the ocean can be both rapid (10^3 - 10^4 y), occurring during or shortly after salt giant formation, as is largely the case for the MSC, and/or gradual ($\gg 10^6$ y) where dissolution occurs post burial, as is occurring in Arctic Canada where a ~290-million-year-old gypsum salt giant is now emerging from beneath thawing and eroding permafrost¹⁵².

Constraints on the evaporite-ion flux in addition to the salt giant succession itself are clearly required. One possibility is to use the seawater $[\text{Ca}^{2+}]$ record¹⁵³. To capture perturbations anticipated from salt giant formation, a high-resolution record is required. However, currently only a handful of $[\text{Ca}^{2+}]$ measurements exist for the entire Cenozoic (ironically mainly from evaporite fluid inclusions¹⁵³). These reveal a general decline over the past 100 million years¹⁵³, but are too few to detect a net $[\text{Ca}^{2+}]_{\text{sw}}$ reduction over the MSC duration, let alone the abrupt sub-precessional scale step-like structure that should be evident from evaporite ion extraction and return. By integrating Ca-evaporite formation and weathering processes, coupled carbon and calcium cycle models will provide more mechanistically sound explanations of the links between geological and geochemical cycles, and climate.

Physical processes associated with salt giant formation could also have a potential impact on global climate. Advection of dense, cold and/or salty overflow water from marginal basins strongly influences the oceanic distribution of heat and salt, exerting a powerful influence on thermohaline circulation and deep-water formation¹⁵⁴. In the North Atlantic today, the densest of these overflows emanates from the Mediterranean

Sea¹⁵⁵ depositing a prominent overflow plume that contours around the Iberian margin¹⁵⁶. Sensitivity experiments that exclude present-day Mediterranean-Atlantic exchange result in $\sim 1^\circ$ cooling over the North Atlantic, and a 0.7-2.3 Sv ($1 \text{ Sv} = 10^6 \text{ m}^3\text{s}^{-1}$) reduction in the Atlantic Meridional Overturning Circulation^{154,157}. These results indicate that the negative Mediterranean hydrologic budget, combined with exchange through the Gibraltar Strait, is enough to generate a climatically important high-density water mass today. The outstanding question remains: what role did overflow have in driving Late Miocene climate?

[H1] Summary and future perspectives

In this Review we provide evidence that both geodynamic and eustatic sea-level forcing are crucial for initiating and terminating salt giant formation with a subsidiary role for regional climate. The formation and dissolution of giant calcium sulphate (gypsum and anhydrite) deposits can have global consequences as an episodic driver of carbon cycle changes. Mediterranean overflow was triggered by initial tectonic restriction of Mediterranean-Atlantic exchange as the two pre-Gibraltar marine gateways formed and closed, allowing a Mediterranean-Atlantic density contrast to develop¹⁴⁸. This restriction process occurred at $\sim 8 \text{ Ma}$ ¹⁴⁸ (Fig. 5), and pre-dated evaporite deposition by two million years and persisted after the MSC throughout the Pliocene and Pleistocene¹⁵⁶. Similar dense overflows might be associated with every marginal basin in which a salt giant has formed and, like the MSC, their duration will not have been synchronous with salt giant formation. The impact of these overflows on thermohaline circulation should be a target for future research.

During salt giant formation, marginal basin water density will have been much higher, and evaporite-sediment alternations such as those of MSC successions, indicate fluctuating brine concentrations. However, only during two-way exchange episodes will this produce a high-density overflow plume that could impact thermohaline circulation. Modelling these extreme high-density overflows is challenging because the narrow, shallow marine gateways required for overflows to form are too small to be fully resolvable in current Earth System Models. Instead, numerical models use various parameterisations to mimic overflow mixing in model simulations^{158,159}; none are currently compatible with densities that far exceed contemporary overflow observations¹⁵⁵. Improved

model parameterisation of overflow mixing and development of proxies that allow overflow density reconstruction will be critical to addressing this challenge.

Finally, this Review provides context for the upcoming Land-2-Sea drilling project in 2024. IMAGE (Investigating Miocene Mediterranean-Atlantic Gateway Exchange)¹⁶⁰ will recover 8- to 4-million-year-old sediments from both gateways and the Mediterranean outflow plume in the Atlantic before, during, and after the MSC. The project objective is to identify and quantify the impact of evolving Mediterranean-Atlantic exchange on regional and global environmental change and specifically its potential contribution to cooling during this period, which ultimately resulted in initiation of northern hemisphere glaciation¹¹¹. This drilling project will combine offshore drilling with International Ocean Discovery Program Expedition 401 on either side of the Gibraltar Strait and onshore drilling with the International Continental Scientific Drilling Program in Morocco and Spain, targeting the two precursor Atlantic-Mediterranean marine connections that have been uplifted and preserved on land. IMAGE, the first Land-2-Sea drilling project, offers great scope for addressing the many remaining unknowns outlined here.

[H1] References

1. Camerlenghi, A. & Aloisi, V. Uncovering the Mediterranean salt giant (MEDSALT) - scientific networking as incubator of cross-disciplinary research in Earth sciences. *Eur. Rev.* **28**, 40–61 (2020).
2. Hübscher, C. *et al.* Global look at salt giants. *Eos (Washington DC)* **88**, (2007).
3. Ryan, W. B. F. Decoding the Mediterranean salinity crisis. *Sedimentology* **56**, 95–136 (2009).
4. Haq, B., Gorini, C., Baur, J., Moneron, J. & Rubino, J. Deep Mediterranean's Messinian evaporite giant: how much salt? *Glob. Planet. Change* **184**, 103052 (2020).
5. Wortmann, U. & Paytan, A. Rapid variability of seawater chemistry over the past 130 million years. *Science* **337**, 334–336 (2012).
6. Heida, H. *et al.* Flexural-isostatic reconstruction of the Western Mediterranean during the Messinian Salinity Crisis: implications for water level and basin connectivity. *Bas. Res.* **34**, 50–80 (2022).
7. Urgeles, R. *et al.* New constraints on the Messinian sealevel drawdown from 3D seismic data of the Ebro Margin, western Mediterranean. *Bas. Res.* **23**, 123–145 (2011).
8. Madof, A. S., Bertoni, C. & Lofi, J. Discovery of vast fluvial deposits provides evidence for drawdown during the late Miocene Messinian salinity crisis. *Geology* **47**, 171–174 (2019).
9. Garcia-Castellanos, D. *et al.* Catastrophic flood of the Mediterranean after the Messinian salinity crisis. *Nature* **462**, 778–781 (2009).
10. van Dijk, G. *et al.* A terminal Messinian flooding of the Mediterranean evidenced by contouritic deposits on Sicily. *Sedimentology* **70**, 1195–1223 (2023).
11. Amarathunga, U. *et al.* Sill-controlled salinity contrasts followed post-Messinian flooding of the Mediterranean. *Nat. Geosci.* **15**, 720–725 (2022).
12. Lofi, J. *et al.* Erosional processes and paleo-environmental changes in the Western Gulf of Lions (SW France) during the Messinian Salinity Crisis. *Mar. Geol.* **217**, 1–30 (2005).
13. Rouchy, J. M. & Caruso, A. The Messinian salinity crisis in the Mediterranean basin: a reassessment of the data and an integrated scenario. *Sediment. Geol.* **188–189**, 35–67 (2006).

14. Gvirtzman, Z. *et al.* Intra-Messinian truncation surface in the Levant Basin explained by subaqueous dissolution. *Geology* **45**, 915–918 (2017).
15. Roveri, M. *et al.* The Messinian Salinity Crisis: past and future of a great challenge for marine sciences. *Mar. Geol.* **352**, 25–58 (2014).
16. Lofi, J. *et al.* Refining our knowledge of the Messinian salinity crisis records in the offshore domain through multi-site seismic analysis. *Bull. Soc. Geol. France* **182**, 163–180 (2011).
17. Hilgen, F. J. *et al.* Extending the astronomical (polarity) time scale into the Miocene. *Earth Planet. Sci. Lett.* **136**, 495–510 (1995).
18. Krijgsman, W., Hilgen, F. J., Raffi, I., Sierro, F. J. & Wilson, D. S. Chronology, causes and progression of the Messinian salinity crisis. *Nature* **400**, 652–655 (1999).
19. Sierro, F. J., Hilgen, F. J., Krijgsman, W. & Flores, J. A. The Abad composite (SE Spain): a Messinian reference section for the Mediterranean and the APTS. *Palaeogeogr. Palaeoclimatol. Palaeoecol.* **168**, 141–169 (2001).
20. Natalicchio, M. *et al.* Did late Miocene (Messinian) gypsum precipitate from evaporated marine brines? insights from the Piedmont basin (Italy). *Geology* **42**, 179–182 (2014).
21. Reghizzi, M., Lugli, S., Manzi, V., Rossi, F. P. & Roveri, M. Orbitally forced hydrological balance during the Messinian Salinity Crisis: insights from strontium isotopes ($^{87}\text{Sr}/^{86}\text{Sr}$) in the Vena del Gesso Basin (Northern Apennines, Italy). *Paleoceanogr. Paleoclimatol.* **33**, 716–731 (2018).
22. Topper, R. P. M. & Meijer, P. T. A modeling perspective on spatial and temporal variations in Messinian evaporite deposits. *Mar. Geol.* **336**, 44–60 (2013).
23. Grothe, A. *et al.* Paratethys pacing of the Messinian Salinity Crisis : low salinity waters contributing to gypsum precipitation ? *Earth Planet. Sci. Lett.* **532**, 116029 (2020).
24. Andretto, F. *et al.* High-amplitude water-level fluctuations at the end of the Mediterranean Messinian Salinity Crisis: implications for gypsum formation, connectivity and global climate. *Earth Planet. Sci. Lett.* **595**, 117767 (2022).
25. Raad, F. *et al.* A song of volumes, surfaces and fluxes: the case study of the Central Mallorca Depression (Balearic Promontory) during the Messinian Salinity Crisis. *Basin Research* **35**, 1–27 (2023).
26. Flecker, R. *et al.* Evolution of the Late Miocene Mediterranean-Atlantic gateways and their impact on regional and global environmental change. *Earth Sci. Rev.* **150**, 365–392 (2015).
27. Hilgen, F., Kuiper, K., Krijgsman, W., Snel, E. & Van der Laan, E. Astronomical tuning as the basis for high resolution chronostratigraphy: the intricate history of the Messinian Salinity Crisis. *Stratigraphy* **4**, 231–238 (2007).
28. Krijgsman, W. *et al.* The Gibraltar Corridor : watergate of the Messinian Salinity Crisis. *Mar. Geol.* **403**, 238–246 (2018).
29. Bryden, H. L., Candela, J. & Kinder, T. H. Exchange through the Strait of Gibraltar. *Prog. Oceanogr.* **33**, 201–248 (1994).
30. Capella, W. *et al.* Palaeogeographic evolution of the late Miocene Rifian Corridor (Morocco): reconstructions from surface and subsurface data. *Earth Sci. Rev.* **180**, 37–59 (2018).
31. Booth-Rea, G., Ranero, C. R. & Grevemeyer, I. The Alboran volcanic-arc modulated the Messinian faunal exchange and salinity crisis. *Sci. Rep.* **8**, 13015 (2018).
32. De la Vara, A., Topper, R. P. M., Meijer, P. T. & Kouwenhoven, T. J. Water exchange through the Betic and Rifian corridors prior to the Messinian Salinity Crisis: a model study. *Paleoceanography* **30**, 548–557 (2015).
33. Bulian, F. *et al.* Impact of the Mediterranean-Atlantic connectivity and the late Miocene carbon shift on deep-sea communities in the Western Alboran Basin. *Palaeogeogr. Palaeoclimatol. Palaeoecol.* **589**, 110841 (2022).
34. Kouwenhoven, T. J., Hilgen, F. J. & Van Der Zwaan, G. J. Late Tortonian-early Messinian stepwise disruption of the Mediterranean-Atlantic connections: constraints from benthic foraminiferal and geochemical data. *Palaeogeogr. Palaeoclimatol. Palaeoecol.* **198**, 303–319 (2003).
35. Mayer-Eymar, K. *Catalogue systématique et descriptif des fossiles des terrains tertiaires qui se trouvent du Musée fédéral de Zürich, Zürich.* (1867).
36. Selli, R. Il Messiniano Mayer-Eymar 1867. Proposta di un neostratotipo. *Giornale di Geologia* **28**, 1–33 (1960).
37. Ruggieri, G. The Miocene and later evolution of the Mediterranean Sea. *Aspects of Tethyan Biogeography* 283–290 (1967).
38. Hsü, K., Ryan, W. B. F. & Cita, M. Late Miocene desiccation of the Mediterranean. *Nature* **242**, 240–244 (1973).
39. Ryan, W. B. F. 50th anniversary review of the Mediterranean desiccation hypothesis. *Rivista del Nuovo Cimento*, **46**, 163–291 (2023).

40. Roveri, M. *et al.* Dense shelf water cascading and Messinian Canyons: a new scenario for the Mediterranean salinity crisis. *Am. J. Sci.* **314**, 751–784 (2014).
41. Lugli, S., Manzi, V., Roveri, M. & Schreiber, B. C. The Primary Lower Gypsum in the Mediterranean: a new facies interpretation for the first stage of the Messinian salinity crisis. *Palaeogeogr. Palaeoclimatol. Palaeoecol.* **297**, 83–99 (2010).
42. Stoica, M., Krijgsman, W., Fortuin, A. & Gliozzi, E. Paratethyan ostracods in the Spanish Lago-Mare: more evidence for interbasinal exchange at high Mediterranean sea level. *Palaeogeogr. Palaeoclimatol. Palaeoecol.* **441**, 854–870 (2016).
43. Andreetto, F. *et al.* Freshening of the Mediterranean Salt Giant: controversies and certainties around the terminal (Upper Gypsum and Lago-Mare) phases of the Messinian Salinity Crisis. *Earth Sci. Rev.* **216**, 103577 (2021).
44. Gliozzi, E., Ceci, M. E., Grossi, F. & Ligios, S. Paratethyan ostracod immigrants in Italy during the Late Miocene. *Geobios* **40**, 325–337 (2007).
45. Manzi, V., Lugli, S., Ricci Lucchi, F. & Roveri, M. Deep-water clastic evaporites deposition in the Messinian Adriatic foredeep (northern Apennines, Italy): did the Mediterranean ever dry out? *Sedimentology* **52**, 875–902 (2005).
46. Raad, F., Lofi, J., Maillard, A., Tzevahirtzian, A. & Caruso, A. The Messinian Salinity Crisis deposits in the Balearic Promontory: an undeformed analog of the MSC Sicilian basins?? *Mar. Pet. Geol.* **124**, 104777 (2021).
47. Ochoa, D. *et al.* Messinian Salinity Crisis deposits widespread over the Balearic Promontory: insights from new high-resolution seismic data. *Mar. Pet. Geol.* **66**, 41–54 (2014).
48. Manzi, V. *et al.* The deep-water counterpart of the Messinian Lower Evaporites in the Apennine foredeep: the Fanantello section (Northern Apennines, Italy). *Palaeogeogr. Palaeoclimatol. Palaeoecol.* **251**, 470–499 (2007).
49. de Lange, G. J. & Krijgsman, W. Messinian salinity crisis: a novel unifying shallow gypsum/deep dolomite formation mechanism. *Mar. Geol.* **275**, 273–277 (2010).
50. Manzi, V., Roveri, M., Argnani, A., Cowan, D. & Lugli, S. Large-scale mass-transport deposits recording the collapse of an evaporitic platform during the Messinian salinity crisis (Caltanissetta basin, Sicily). *Sediment. Geol.* **424**, 106003 (2021).
51. Lugli, S., Manzi, V., Roveri, M. & Schreiber, B. C. The deep record of the Messinian salinity crisis: evidence of a non-desiccated Mediterranean Sea. *Palaeogeogr. Palaeoclimatol. Palaeoecol.* **433**, 201–218 (2015).
52. Gvirtzman, Z., Reshef, M., Buch-Leviatan, O. & Ben-Avraham, Z. Intense salt deformation in the Levant Basin in the middle of the Messinian Salinity Crisis. *Earth Planet. Sci. Lett.* **379**, 108–119 (2013).
53. Bertoni, C. & Cartwright, J. A. Controls on the basinwide architecture of late Miocene (Messinian) evaporites on the Levant margin (Eastern Mediterranean). *Sediment. Geol.* **188–189**, 93–114 (2006).
54. Feng, Y. E., Steinberg, J. & Reshef, M. Intra-salt deformation: Implications for the evolution of the Messinian evaporites in the Levant Basin, eastern Mediterranean. *Mar. Pet. Geol.* **88**, 251–267 (2017).
55. Feng, Y. E., Yankelzon, A., Steinberg, J. & Reshef, M. Lithology and characteristics of the Messinian evaporite sequence of the deep Levant Basin, Eastern Mediterranean. *Mar. Geol.* **376**, 118–131 (2016).
56. Manzi, V. *et al.* Synchronous onset of the Messinian salinity crisis and diachronous evaporite deposition: new evidences from the deep Eastern Mediterranean basin. *Palaeogeogr. Palaeoclimatol. Palaeoecol.* **584**, 110685 (2021).
57. Manzi, V., Lugli, S., Roveri, M., Schreiber, B. C. & Gennari, R. The Messinian ‘Calcere di Base’ (Sicily, Italy) revisited. *Bull. Geol. Soc. Am.* **123**, 347–370 (2011).
58. Caruso, A., Pierre, C., Blanc-Valleron, M.-M. & Rouchy, J. M. Carbonate deposition and diagenesis in evaporitic environments: the evaporative and sulphur-bearing limestones during the settlement of the Messinian Salinity Crisis in Sicily and Calabria. *Palaeogeogr. Palaeoclimatol. Palaeoecol.* **429**, 136–162 (2015).
59. Bourillot, R. *et al.* Structure and evolution of a Messinian mixed carbonate-siliciclastic platform: the role of evaporites (Sorbas Basin, South-East Spain). *Sedimentology* **57**, 477–512 (2010).
60. Roveri, M., Lugli, S., Manzi, V., Reghizzi, M. & Rossi, F. P. Stratigraphic relationships between shallow-water carbonates and primary gypsum: insights from the Messinian succession of the Sorbas Basin (Betic Cordillera, Southern Spain). *Sediment. Geol.* **404**, 105678 (2020).
61. Roveri, M., Lugli, S., Manzi, V. & Schreiber, B. C. The Messinian Sicilian stratigraphy revisited: new insights for the Messinian salinity crisis. *Terra Nova* **20**, 483–488 (2008).
62. Manzi, V. *et al.* High-frequency cyclicity in the Mediterranean Messinian evaporites: evidence for solar-lunar climate forcing. *J. Sediment. Res.* **82**, 991–1005 (2012).

63. García-Veigas, J., Cendón, D. I., Gibert, L., Lowenstein, T. K. & Artiaga, D. Geochemical indicators in Western Mediterranean Messinian evaporites: implications for the salinity crisis. *Mar. Geol.* **403**, 197–214 (2018).
64. Bulian, F., Kouwenhoven, T. J., Andersen, N., Krijgsman, W. & Sierro, F. J. Reflooding and repopulation of the Mediterranean Sea after the Messinian Salinity Crisis: benthic foraminifera assemblages and stable isotopes of Spanish basins. *Mar. Micropal.* **176**, 102160 (2022).
65. Rohling, E. J., Marino, G. & Grant, K. M. Mediterranean climate and oceanography, and the periodic development of anoxic events (sapropels). *Earth Sci. Rev.* **143**, 62–97 (2015).
66. Manzi, V. *et al.* Age refinement of the Messinian salinity crisis onset in the Mediterranean. *Terra Nova* **25**, 315–322 (2013).
67. Zachariasse, W. J. & Lourens, L. J. The Messinian on Gavdos (Greece) and the status of currently used ages for the onset of the MSC and gypsum precipitation. *Newsl. Stratigr.* **55**, 333–360 (2022).
68. Tzevahirtzian, A., Caruso, A., Andreetto, F., Bonomo, S. & Krijgsman, W. A bio-chronostratigraphic study of the upper Miocene from the northern Caltanissetta Basin, Sicily (core 3AGN2S04). Implications for dating the Messinian Salinity Crisis onset. *Sediment. Geol.* **445**, (2023).
69. Van Couvering, J. A., Castradori, D., Cita, M. B., Hilgen, F. J. & Rio, D. The base of the Zanclean Stage and of the Pliocene Series. *Episodes* **23**, 179–187 (2000).
70. Clauzon, G., Suc, J.-P., Gautier, F., Berger, A. & Loutre, M.-F. Alternate interpretation of the Messinian salinity crisis: Controversy resolved? *Geology* **24**, 363–366 (1996).
71. Krijgsman, W. *et al.* Revised astrochronology for the Ain el Beida section (Atlantic Morocco): no glacio-eustatic control for the onset of the Messinian Salinity Crisis. *Stratigraphy* **1**, 87–101 (2004).
72. Topper, R. P. M., Flecker, R., Meijer, P. T. & Wortel, M. J. R. A box model of the Late Miocene Mediterranean Sea: implications from combined $^{87}\text{Sr}/^{86}\text{Sr}$ and salinity data. *Paleoceanography* **26**, PA3223 (2011).
73. Krijgsman, W., Fortuin, A. R., Hilgen, F. J. & Sierro, F. J. Astrochronology for the Messinian Sorbas basin (SE Spain) and orbital (precessional) forcing for evaporite cyclicity. *Sediment. Geol.* **140**, 43–60 (2001).
74. Rohling, E. J., Schiebel, R. & Siddall, M. Controls on Messinian Lower Evaporite cycles in the Mediterranean. *Earth Planet. Sci. Lett.* **275**, 165–171 (2008).
75. Garcia-Castellanos, D. & Villaseñor, A. Messinian salinity crisis regulated by competing tectonics and erosion at the Gibraltar arc. *Nature* **480**, 359–363 (2011).
76. Krijgsman, W. & Meijer, P. T. Depositional environments of the Mediterranean “Lower Evaporites” of the Messinian salinity crisis: constraints from quantitative analyses. *Mar. Geol.* **253**, 73–81 (2008).
77. Manzi, V. *et al.* The onset of the Messinian salinity crisis in the deep Eastern Mediterranean basin. *Terra Nova* **30**, 189–198 (2018).
78. Meilijson, A. *et al.* Chronology with a pinch of salt: integrated stratigraphy of Messinian evaporites in the deep Eastern Mediterranean reveals long-lasting halite deposition during Atlantic connectivity. *Earth Sci. Rev.* **194**, 374–398 (2019).
79. Meijer, P. T. A box model of the blocked-outflow scenario for the Messinian Salinity Crisis. *Earth Planet. Sci. Lett.* **248**, 486–494 (2006).
80. Sanford, W. E. & Wood, W. W. Brine evolution and mineral deposition in hydrologically open evaporite basins. *Am. J. Sci.* **291**, 687–710 (1991).
81. Manzi, V., Lugli, S., Roveri, M. & Schreiber, B. C. A new facies model for the Upper Gypsum of Sicily (Italy): chronological and palaeoenvironmental constraints for the Messinian salinity crisis in the Mediterranean. *Sedimentology* **56**, 1937–1960 (2009).
82. Andreetto, F. *et al.* Multi-proxy investigation of the post-evaporitic succession of the Piedmont Basin (Pollenzo section, NW Italy): a new piece in the Stage 3 puzzle of the Messinian Salinity Crisis. *Palaeogeogr. Palaeoclimatol. Palaeoecol.* **594**, 110961 (2022).
83. Jolivet, L., Augier, R., Robin, C., Suc, J.-P. & Rouchy, J. M. Lithospheric-scale geodynamic context of the Messinian salinity crisis. *Sediment. Geol.* **188–189**, 9–33 (2006).
84. Mancilla, F. L. *et al.* Slab rupture and delamination under the Betics and Rif constrained from receiver functions. *Tectonophysics* **663**, 225–237 (2015).
85. Spakman, W., Chertova, M. V., Van Den Berg, A. & Van Hinsbergen, D. J. J. Puzzling features of western Mediterranean tectonics explained by slab dragging. *Nat. Geosci.* **11**, 211–216 (2018).
86. Wortel, M. J. R. & Spakman, W. Subduction and slab detachment in the Mediterranean-Carpathian region. *Science* **290**, 1910–1917 (2000).
87. Capella, W., Spakman, W., van Hinsbergen, D. J. J., Chertova, M. V. & Krijgsman, W. Mantle resistance against Gibraltar slab dragging as a key cause of the Messinian Salinity Crisis. *Terra Nova* **32**, 141–150 (2020).

88. Capella, W. *et al.* Thick-skinned tectonics closing the Rifian Corridor. *Tectonophysics* **710–711**, 249–265 (2017).
89. Sabino, M. *et al.* Climatic and hydrologic variability in the northern Mediterranean across the onset of the Messinian salinity crisis. *Palaeogeogr. Palaeoclimatol. Palaeoecol.* **545**, 109632 (2020).
90. Modestou, S. *et al.* Precessional variability of $^{87}\text{Sr}/^{86}\text{Sr}$ in the late Miocene Sorbas Basin: an interdisciplinary study of drivers of interbasin exchange. *Paleoceanography* **32**, 531–552 (2017).
91. Blanc, P.-L. Of sills and straits: a quantitative assessment of the Messinian Salinity Crisis. *Deep Sea Res. I Oceanogr. Res. Pap.* **47**, 1429–1460 (2000).
92. Meijer, P. & Krijgsman, W. A quantitative analysis of the desiccation and re-filling of the Mediterranean during the Messinian Salinity Crisis. *Earth Planet. Sci. Lett.* **240**, 510–520 (2005).
93. Pellen, R. *et al.* Structural and sedimentary origin of the Gargano – Pelagosa gateway and impact on sedimentary evolution during the Messinian Salinity Crisis. *Earth Sci. Rev.* **232**, 104114 (2022).
94. Krijgsman, W., Palcu, D. V., Andreotto, F., Stoica, M. & Mandic, O. Changing seas in the late Miocene Northern Aegean: a Paratethyan perspective to Mediterranean stratigraphy. *Earth Sci. Rev.* **210**, 103386 (2020).
95. Gülyüz, E., Durak, H., Özkaptan, M. & Krijgsman, W. Paleomagnetic constraints on the early Miocene closure of the southern Neo-Tethys (Van region; East Anatolia): inferences for the timing of Eurasia- Arabia collision. *Glob. Planet. Change* **185**, 103089 (2020).
96. Harzhauser, M., Piller, W. E. & Steininger, F. F. Circum-Mediterranean Oligo–Miocene biogeographic evolution – the gastropods’ point of view. *Palaeogeogr. Palaeoclimatol. Palaeoecol.* **183**, 103–133 (2002).
97. Oguz, T., Özsoy, E., Latif, M. A., Sur, H. I. & Ünlüata, Ü. Modeling of hydraulically controlled exchange flow in the Bosphorus Strait. *J. Phys. Oceanogr.* **20**, 945–965 (1990).
98. Radionova, E. P. & Golovina, L. Upper Maeotian-Lower Pontian ‘Transitional Strata’ in the Taman Peninsula: stratigraphic position and paleogeographic interpretation. *Geol. Carpath.* **62**, 77–90 (2011).
99. Grothe, A., Sangiorgi, F., Brinkhuis, H., Stoica, M. & Krijgsman, W. Migration of the dinoflagellate *Galeacysta etrusca* and its implications for the Messinian Salinity Crisis. *Newsl. Stratigr.* **51**, 73–91 (2018).
100. Van Baak, C. G. C., Stoica, M., Grothe, A., Aliyeva, E. & Krijgsman, W. Mediterranean-Paratethys connectivity during the Messinian salinity crisis: the Pontian of Azerbaijan. *Glob. Planet. Change* **141**, 63–81 (2016).
101. Van Baak, C. G. C. *et al.* Paratethys response to the Messinian salinity crisis. *Earth Sci. Rev.* **172**, 193–223 (2017).
102. Krijgsman, W. *et al.* Mediterranean-Black Sea gateway exchange: Scientific drilling workshop on the BlackGate project. *Sci. Drill.* **31**, 93–110 (2022).
103. Wegwerth, A. *et al.* Meltwater events and the Mediterranean reconnection at the Saalian–Eemian transition in the Black Sea. *Earth Planet. Sci. Lett.* **404**, 124–135 (2014).
104. Bista, D. *et al.* Sr isotope-salinity modelling constraints on Quaternary Black Sea connectivity. *Quat. Sci. Rev.* **273**, 107254 (2021).
105. Westerhold, T. *et al.* An astronomically dated record of Earth’s climate and its predictability over the last 66 million years. *Science* **369**, 1383–1388 (2020).
106. Ohneiser, C. *et al.* Antarctic glacio-eustatic contributions to late Miocene Mediterranean desiccation and reflooding. *Nat. Commun.* **6**, 8765 (2015).
107. Rohling, E. J. *et al.* Comparison and synthesis of sea-level and deep-sea temperature variations over the past 40 million years. *Reviews of Geophysics* **60**, e2002RG000775 (2022).
108. Gladstone, R., Flecker, R., Valdes, P., Lunt, D. & Markwick, P. The Mediterranean hydrologic budget from a Late Miocene global climate simulation. *Palaeogeogr. Palaeoclimatol. Palaeoecol.* **251**, 254–267 (2007).
109. Simon, D. *et al.* Quantifying the Mediterranean freshwater budget throughout the late Miocene: new implications for sapropel formation and the Messinian Salinity Crisis. *Earth Planet. Sci. Lett.* **472**, 25–37 (2017).
110. Drury, A. J. *et al.* Late Miocene climate and time scale reconciliation: accurate orbital calibration from a deep-sea perspective. *Earth Planet. Sci. Lett.* **475**, 254–266 (2017).
111. Herbert, T. D. *et al.* Late Miocene global cooling and the rise of modern ecosystems. *Nat. Geosci.* **9**, 843–847 (2016).
112. van der Laan, E. *et al.* Astronomical forcing of Northwest African climate and glacial history during the late Messinian (6.5–5.5Ma). *Palaeogeogr. Palaeoclimatol. Palaeoecol.* **313–314**, 107–126 (2012).
113. Holbourn, A. E. *et al.* Late Miocene climate cooling and intensification of southeast Asian winter monsoon. *Nat. Commun.* **9**, (2018).
114. Kontakiotis, G. *et al.* Decoding sea surface and paleoclimate conditions in the eastern Mediterranean over the Tortonian-Messinian Transition. *Palaeogeogr. Palaeoclimatol. Palaeoecol.* **534**, 109312 (2019).

115. Bulian, F., Sierro, F. J., Ledesma, S., Jiménez-Espejo, F. J. & Bassetti, M.-A. Messinian West Alboran Sea record in the proximity of Gibraltar: early signs of Atlantic-Mediterranean gateway restriction. *Mar. Geol.* **434**, 106430 (2021).
116. Sabino, M. *et al.* Climatic and hydrologic variability in the northern Mediterranean across the onset of the Messinian salinity crisis. *Palaeogeogr. Palaeoclimatol. Palaeoecol.* **545**, 109632 (2020).
117. Natalicchio, M. *et al.* Paleoenvironmental change in a precession-paced succession across the onset of the Messinian salinity crisis: insight from element geochemistry and molecular fossils. *Palaeogeogr. Palaeoclimatol. Palaeoecol.* **518**, 45–61 (2019).
118. Rohling, E. J. *et al.* Sea level and deep-sea temperature reconstructions suggest quasi-stable states and critical transitions over the past 40 million years. *Sci. Adv.* **7**, eabf5326 (2021).
119. Fauquette, S. *et al.* How much did climate force the Messinian salinity crisis? Quantified climatic conditions from pollen records in the Mediterranean region. *Palaeogeogr. Palaeoclimatol. Palaeoecol.* **238**, 281–301 (2006).
120. Vasiliev, I. *et al.* How dry was the Mediterranean during the Messinian salinity crisis? *Palaeogeogr. Palaeoclimatol. Palaeoecol.* **471**, 120–133 (2017).
121. Butiseacă, G. A. *et al.* Multiple crises preceded the Mediterranean Salinity Crisis: aridification and vegetation changes revealed by biomarkers and stable isotopes. *Glob. Planet. Change* **217**, 103951 (2022).
122. Karakitsios, V. *et al.* Messinian salinity crisis record under strong freshwater input in marginal, intermediate, and deep environments : the case of the North Aegean. *Palaeogeogr. Palaeoclimatol. Palaeoecol.* **485**, 316–335 (2017).
123. Kontakiotis, G. *et al.* Hypersalinity accompanies tectonic restriction in the eastern Mediterranean prior to the Messinian Salinity Crisis. *Palaeogeogr. Palaeoclimatol. Palaeoecol.* **592**, 110903 (2022).
124. Bertini, A. The Northern Apennines palynological record as a contribute for the reconstruction of the Messinian palaeoenvironments. *Sediment. Geol.* **188–189**, 235–258 (2006).
125. Hilgen, F. J. Astronomical calibration of Gauss to Matuyama sapropels in the Mediterranean and implication for the Geomagnetic Polarity Time Scale. *Earth Planet. Sci. Lett.* **104**, 226–244 (1991).
126. Marzocchi, A. *et al.* Orbital control on late Miocene climate and the North African monsoon: insight from an ensemble of sub-precessional simulations. *Clim. Past* **11**, 1271–1295 (2015).
127. Larrasoaña, J. C., Roberts, A. P. & Rohling, E. J. Dynamics of Green Sahara Periods and their role in hominin evolution. *PLoS One* **8**, e76514 (2013).
128. Grant, K. M. *et al.* Organic carbon burial in Mediterranean sapropels intensified during Green Sahara Periods since 3.2 Myr ago. *Commun. Earth Environ.* **3**, (2022).
129. Colin, C. *et al.* Reconstruction of Northern African monsoon between 6.2 and 4.9 Ma and possible relationships with Late Miocene events. *C. R. Geosci.* **340**, 749–760 (2008).
133. Colin, C. *et al.* Late Miocene to early Pliocene climate variability off NW Africa (ODP Site 659). *Palaeogeogr. Palaeoclimatol. Palaeoecol.* **401**, 81–95 (2014).
131. Krijgsman, W., Stoica, M., Vasiliev, I. & Popov, V. V. Rise and fall of the Paratethys Sea during the Messinian Salinity Crisis. *Earth Planet. Sci. Lett.* **290**, 183–191 (2010).
132. Palcu, D. V. *et al.* Late Miocene megalake regressions in Eurasia. *Sci. Rep.* **11**, 1–12 (2021).
133. Sprovieri, M., Sacchi, M. & Rohling, E. J. Climatically influenced interactions between the Mediterranean and the Paratethys during the Tortonian. *Paleoceanography* **18**, 1034 (2003).
134. Amies, J. D., Rohling, E. J., Grant, K. M., Rodríguez-Sanz, L. & Marino, G. Quantification of African monsoon runoff during last interglacial sapropel S5. *Paleoceanogr. Paleoclimatol.* **34**, 1487–1516 (2019).
135. Bosmans, J. H. C. *et al.* Precession and obliquity forcing of the freshwater budget over the Mediterranean. *Quat. Sci. Rev.* **123**, 16–30 (2015).
136. Griffin, D. L. The late Neogene Sahabi rivers of the Sahara and their climatic and environmental implications for the Chad Basin. *J. Geol. Soc. London* **163**, 905–921 (2006).
137. Griffin, D. L. Aridity and humidity: two aspects of the late Miocene climate of North Africa and the Mediterranean. *Palaeogeogr. Palaeoclimatol. Palaeoecol.* **182**, 65–91 (2002).
138. Drake, N. A. *et al.* Reconstructing palaeoclimate and hydrological fluctuations in the Fezzan Basin (southern Libya) since 130 ka: a catchment-based approach. *Quat. Sci. Rev.* **200**, 376–394 (2018).
139. Rohling, E. J. *et al.* African monsoon variability during the previous interglacial maximum. *Earth Planet. Sci. Lett.* **202**, 61–75 (2002).
140. Coulthard, T. J., Ramirez, J. A., Barton, N., Rogerson, M. & Brücher, T. Were rivers flowing across the Sahara during the last interglacial? implications for human migration through Africa. *PLoS One* **8**, e74834 (2013).
141. Aloisi, G. *et al.* The geochemical riddle of “low-salinity gypsum” deposits. *Geochim. Cosmochim. Acta* **327**, 247–275 (2022).

142. Wallmann, K. *et al.* Salty brines on the Mediterranean sea floor. *Nature* **387**, 31–32 (1997).
143. La Cono, V. *et al.* The discovery of Lake Hephæstus, the youngest athalassohaline deep-sea formation on Earth. *Sci. Rep.* **9**, 1679 (2019).
144. Yakimov, M. M. *et al.* Microbial community of the deep-sea brine Lake Kryos seawater-brine interface is active below the chaotricity limit of life as revealed by recovery of mRNA. *Environ. Microbiol.* **17**, 364–382 (2015).
145. Warren, J. K. Evaporites through time: tectonic, climatic and eustatic controls in marine and nonmarine deposits. *Earth Sci. Rev.* **98**, 217–268 (2010).
146. Shields, G. A. & Mills, B. J. W. Evaporite weathering and deposition as a long-term climate forcing mechanism. *Geology* **49**, 299–303 (2021).
147. Hay, W. W. *et al.* Evaporites and the salinity of the ocean during the Phanerozoic: implications for climate, ocean circulation and life. *Palaeogeogr. Palaeoclimatol. Palaeoecol.* **240**, 3–46 (2006).
148. Capella, W. *et al.* Mediterranean isolation preconditioning the Earth System for late Miocene climate cooling. *Sci. Rep.* **9**, 3795 (2019).
149. Berner, R. A. A model for atmospheric CO₂ over Phanerozoic time. *Am. J. Sci.* **291**, 339–376 (1991).
150. Lenton, T. M., Daines, S. J. & Mills, B. J. W. COPSE reloaded: an improved model of biogeochemical cycling over Phanerozoic time. *Earth Sci. Rev.* **178**, 1–28 (2018).
151. Nichols, G., Williams, E. & Paola, C. *Sedimentary Processes, Environments and Basins*. (Blackwell Publishing Ltd., Oxford, UK, 2007).
152. Hamilton, J. & Ford, D. Karst geomorphology and hydrogeology of the Bear Rock Formation - a remarkable dolostone and gypsum megabreccia in the continuous permafrost zone of northwest territories, Canada. *Carbonates Evaporites* **17**, 114–115 (2002).
153. Turchyn, A. V. & De Paolo, D. J. *Seawater Chemistry through Phanerozoic Time*. *Annu. Rev. Earth Planet. Sci.* **47**, 197–224 (2019).
154. Ivanovic, R. F., Valdes, P. J., Gregoire, L., Flecker, R. & Gutjahr, M. Sensitivity of modern climate to the presence, strength and salinity of Mediterranean-Atlantic exchange in a global general circulation model. *Clim. Dyn.* **42**, 859–877 (2014).
155. Legg, S. *et al.* Improving oceanic overflow representation in climate models: the Gravity Current Entrainment Climate Process Team. *Bull. Am. Meteorol. Soc.* **90**, 657–670 (2009).
156. Hernández-Molina, F. J. *et al.* Onset of Mediterranean outflow into the North Atlantic. *Science* **344**, 1244–1250 (2014).
157. Bigg, G. R., Jickells, T. D., Liss, P. S. & Osborn, T. J. The role of the oceans in climate. *Int. J. Climatol.* **23**, 1127–1159 (2003).
158. Adcroft, A. *et al.* The GFDL Global Ocean and Sea Ice Model OM4.0: Model Description and Simulation Features. *J. Adv. Model. Earth Syst.* **11**, 3167–3211 (2019).
159. Bruciaferri, D., Shapiro, G. I. & Wobus, F. A multi-envelope vertical coordinate system for numerical ocean modelling. *Ocean Dyn.* **68**, 1239–1258 (2018).
160. Flecker, R. https://iodp.tamu.edu/scienceops/expeditions/mediterranean_atlantic_gateway_exchange.html. (2022).
161. Dumitru, O. A. *et al.* Constraints on global mean sea level during Pliocene warmth. *Nature* **574**, 233–236 (2019).
162. Dumitru, O. A. *et al.* Sea-level stands from the Western Mediterranean over the past 6.5 million years. *Sci. Rep.* **11**, 261 (2021).
163. Hollyday, A. *et al.* A revised estimate of Early Pliocene global mean sea level using geodynamic models of the Patagonian slab window. *Geochem., Geophys., Geosyst.* **24**, e2022GC010648 (2023).
164. Bryden, H. L. & Kinder, T. H. Steady two-layer exchange through the Strait of Gibraltar. *Deep-Sea Res.* **38** (Suppl. 1), S445–S463 (1991).
165. Popov, S. V. *et al.* Late Miocene to Pliocene palaeogeography of the Paratethys and its relation to the Mediterranean. *Palaeogeogr. Palaeoclimatol. Palaeoecol.* **238**, 91–106 (2006).
166. Laskar, J. *et al.* A long-term numerical solution for the insolation quantities of the Earth. *Astron. Astrophys.* **428**, 261–285 (2004).
167. Hilgen, F. J., Lourens, L. J. & Van Dam, J. A. The Neogene Period. in *The Geological Time Scale 2012* (eds. Gradstein, F. M., Ogg, J. G., Schmitz, M. D. & Ogg, G. M.) 947–1002 (Elsevier B.V., Amsterdam, 2012).
168. Lisiecki, L. E. & Raymo, M. E. A Pliocene-Pleistocene stack of 57 globally distributed benthic δ¹⁸O records. *Paleoceanography* **20**, 1–17 (2005).
169. Lowenstein, T. K., Timofeeff, M. N., Brennan, S. T., Hardie, L. A. & Demicco, R. V. Oscillations in Phanerozoic seawater chemistry: evidence from fluid Inclusions. *Science* **294**, 1086–1088 (2001).

170. Babel, M. & Schreiber, B. C. *Geochemistry of evaporites and evolution of seawater. Treatise on Geochemistry: Second Edition* vol. 9 (2014).
171. Harvie, C. E. & Weare, J. H. The prediction of mineral solubilities in natural waters: the Na-K-Mg-Ca-Cl-SO₄-H₂O system from zero to high concentration at 25°C. *Geochim. Cosmochim. Acta* **44**, 723–751 (1980).
172. Gaillardet, J., Dupré, B., Louvat, P. & Allègre, C. J. Global silicate weathering and CO₂ consumption rates deduced from the chemistry of large rivers. *Chem. Geol.* **159**, 3–30 (1999).
173. Meybeck, M. Global analysis of river systems: From Earth system controls to Anthropocene syndromes. *Phil. Trans. R. Soc. Lond.* **358**, 1935–1955 (2003).

Supplementary Note

We constructed a sea-level record relative to the present level (0 m) for the 7.5 to 5.0 Ma time interval from the synthesis of Rohling et al.¹⁰⁷. We include sea-level benchmarks from Mallorcan marine cave deposits and Patagonian coastal deposits, which have been corrected for tectonic changes, glacio-isostatic effects, and dynamic topography^{161–163}, and which corroborate the sea-level record from benthic δ¹⁸O deconvolution before, and across, the Miocene-Pliocene boundary. Water exchange thresholds were calculated using the channel geometries of Krijgsman et al.²⁸, which we combine into an approximately triangular single width vs. depth profile (maximum width = 3.28 km; maximum depth = 136 m). Today, the Gibraltar Strait is 10.67 km wide at sea level with 136 m of water above the sill. Hence, the triangular cross-sectional area of the Messinian strait was 3.25 times more restricted than the modern triangular cross-sectional strait area for the same depth. We use this extra restriction in the Bryden and Kinder¹⁶⁴ model for water exchange through the strait, ignoring friction and assuming that excess evaporation (= evaporation – precipitation – runoff) over the basin was equal to that at present. We then calculate water depths in the Messinian strait required for key basin salinity thresholds of 350 (halite), 135 (gypsum), and ~75 ppt (evaporative carbonate); this yields depths of 13 m, 22 m, and 41 m, respectively.

Acknowledgements

This research was supported by the project SALTGIANT-Understanding the Mediterranean Salt Giant, funded by the European Union's Horizon 2020 program (Marie Skłodowska-Curie grant agreement No 765256). It also contributes to Australian Research Council projects FL120100050, DP2000101157 (E.J.R.), and DP190100874 (A.P.R.). D.V.P acknowledges project PNRR C9 - I8 "Multiproxy reconstruction of Eurasian Megalakes, connectivity and isolation patterns during Neogene-Quaternary times", code 97/15.11.2022, Contract No. 760115/23.05.2023 and the project "Impact of sea-level rise on anoxic basins: Paratethys vs. Black Sea" [grant Veni.212.136] of the research Talent programmed – Veni which is financed by the Dutch Research Council (NWO).

Competing interests

The authors declare no competing interests.

Author contributions

All authors contributed to the content, discussion, writing, and editing of the paper. DP, FR, VA, FS, EJR, and UA constructed the figures.

Peer review information

Nature Reviews Earth & Environment thanks [Referee#1 name], [Referee#2 name] and the other, anonymous, reviewer(s) for their contribution to the peer review of this work.

Publisher's note

Springer Nature remains neutral with regard to jurisdictional claims in published maps and institutional affiliations.

Data availability

The data for figures X, Y, and Z are available ...

Supplementary information

Supplementary information is available for this paper at <https://doi.org/10.1038/s415XX-XXX-XXXX-X>

Figures

Figure 1. Mediterranean MSC evaporite stages. a | Map of the Mediterranean region with the most important seas, straits, and mountain ranges labelled. *b-d* | Schematic maps of the Mediterranean and Paratethys seas during three evaporite stages¹⁵ with the main sites that crop out onshore. *b* | Non-marine upper gypsum (UG) stage with lacustrine deposits and Paratethyan fauna known as the “Lago Mare” in Mediterranean highstands and evaporites in lowstands; *c* | the desiccation stage during which halite was deposited; and *d* | water level during the marine primary lower gypsum (PLG) stage with Atlantic connectivity. For detailed distribution patterns from both offshore seismic and onshore field data, see refs.^{3,4,12–14,16,46,94,165}. This series of maps illustrates the sequence of evaporite units that define the MSC during which the Mediterranean became restricted and isolated from the Atlantic .

Figure 2. MSC stratigraphy in basinal settings. A | Schematic Mediterranean map of Messinian marginal zones (MZ), shallow silled basins (SSB), intermediate basins (IB) and central deep basins (CDB). *B* | Schematic Mediterranean cross-section with MSC deposits in different basin settings. The numbers in the layers refer to: 1 - Primary Lower Gypsum (PLG) phase; 2 – Halite; 3 - Upper Gypsum (UG) phase. *C* | Age constraints and distribution of MSC deposits in different basin settings. The complexity of MSC stratigraphic records is illustrated based on depth and tectonic setting.

Figure 3. Global benthic foraminiferal oxygen and carbon isotope records correlated to the main MSC phases. **a** | Messinian magnetic polarity pattern. **b** | Messinian stratigraphic units. UG= Upper Gypsum, with 7 gypsum layers (white) interbedded with mudstones (grey)²⁴, PLG=Primary Lower Gypsum with 16 gypsum layers (white) interbedded with mudstones^{15,27}. Precession-driven sedimentary cycles during the pre-evaporite stage: LA1 to LA21 and UA1 to UA34 indicate Lower and Upper Abad sedimentary cycles¹⁹ (the thickness of each sedimentary cycle has been adjusted to its time span)⁶⁷. Legend for the pre-evaporite cycles: pink, white, black and beige levels indicate indurated layers, homogeneous marls, sapropels and diatomaceous marls, respectively. **c** | Insolation at 65°N for 21 June (black curve)¹⁶⁶. **d** | Changes in Earth's orbital eccentricity (red curve)¹⁶⁶. **e** | Benthic foraminiferal $\delta^{18}\text{O}$ from ODP Site 982 (North Atlantic)¹¹⁰. **f** | Changes in Earth's tilt through the Messinian (red line)¹⁶⁶. **g** | Cenozoic benthic foraminiferal $\delta^{18}\text{O}$ reference record¹⁰⁵. **h** | Cenozoic benthic foraminiferal $\delta^{13}\text{C}$ reference record¹⁰⁵. LMCIS: Late Miocene Carbon Isotope Shift. **i** | Northern Hemispheric sea surface temperature (SST, black line) stack and tropical sea surface temperature stack (yellow line)¹¹¹. The scale reflects the difference in temperature from the present (note that the two SST scales are different). **j** | Messinian Geomagnetic Polarity Time Scale^{105,110}. Vertical light-teal bands: main late Messinian global glacial isotope stages. Dashed vertical lines: main restriction steps for Atlantic-Mediterranean water exchange; the upper one results in the PLG onset. Red arrows indicate gypsum beds deposited during insolation minima. This figure is a summary of Mediterranean Messinian cyclostratigraphy that provides a detailed MSC chronology and a basis to correlate MSC events to global chronostratigraphic records.

Figure 4. Sea-level reconstruction with MSC sill-depth scenarios. **a** | Sea-level relative to present day over the last 10 Myr. The Plio-Pleistocene record (red) is based on benthic $\delta^{18}\text{O}$ deconvolution^{107,118} using combined compilations from refs.¹⁶⁸ and ¹⁰⁵. For the Miocene (blue), we use the envelope between the main benthic $\delta^{18}\text{O}$ deconvolution and sensitivity scenario i of ref.¹⁰⁷ (see that study for rationale and details) based ¹⁰⁵on the benthic $\delta^{18}\text{O}$ compilation of ref.¹⁰⁵. Sea-level benchmarks are also shown for Mallorcan marine cave deposits (black circles with error bars) and Patagonian coastal deposits (grey box), which have been corrected for tectonic changes, glacio-isostatic effects, and dynamic topography¹⁶¹⁻¹⁶³. **b** | Detail of the records from **a** between 5 and 6.4 Ma. We compare sea-level variations with the likely Atlantic-Mediterranean gateway geometry and calculate threshold values for water exchange through the strait that delimit precipitation of halite (H), gypsum (G), evaporative carbonate (EC), or hemipelagic marl deposition (M), as detailed in the Supplementary Note. The inferred MSC sill (grey shading) scenario assumes a disconnected (drawn down) condition during halite and UG deposition. MSC phases are coloured as in Figure 3. Purple up arrows indicate potential gypsum phases in the PLG, and green down arrows indicate ~7 potential (mostly continental) gypsum phases in the UG. From this sea level reconstruction it can be seen that eustatic sea level change was not a primary cause of the onset or end of the MSC, although seawater influxes over the sill during sea level highstands provided the water and ion resupply needed for ongoing evaporite formation.

Figure 5. Geodynamic context of the MSC. **a** | Schematic topography of the pre-MSC Gibraltar region with palaeogeographic projection of Mediterranean-Atlantic gateways. The labels illustrate the timing and mechanisms of vertical motion that restricted Atlantic-Mediterranean connectivity (~5.33–7 Ma). **b** | Cartoon of slab morphology below Gibraltar at ~8 Ma. Arrows illustrate absolute plate motions for Africa and Iberia with slower central-eastern Betic motion. Panel a adapted from ref.⁸⁷, CC BY 4.0. Panel b adapted from.⁸⁵, Springer Nature Limited. The Messinian landmass configuration required for Atlantic-Mediterranean connection or restriction was controlled by Africa-Iberia convergence and the illustrated geodynamics.

Figure 6. Post-MSC removal of Messinian salts to the Atlantic, following an abrupt refilling event. **a** | Sketch of the Mediterranean configuration immediately following abrupt basin refilling by Atlantic waters. The energetic Atlantic inflow transferred almost all western Mediterranean Messinian salt to the Eastern basin, which became stratified with salts to the Sicily sill level. Turbulent diffusion of salts from the lower dense layer (driven by energy input from winds and tides) slowly transferred Messinian salts back to the Atlantic across the Sicily and Camarinal sills, via the outflow. **b** | Timescale of complete salt removal (grey box: 10-40 kyr) for turbulent diffusivities of $1-5 \times 10^{-5} \text{ m}^2\text{s}^{-1}$. The shaded area between the K_1 and K_5 curves represents all possible bottom water salinity reduction pathways. t_{k1} , t_{k5} = time taken to reach surface salinity values at K_1

and K_5 turbulent diffusivities, respectively. S_{LIW} = Levantine intermediate water salinity. Panel b adapted from ref.¹¹, Springer Nature Limited. Illustration of how Atlantic inflow at Gibraltar at the MSC termination first filled the western basin then cascaded into the eastern basin at the Sicily sill to fill it with dense brines that required 26,000 years to flush back to the Atlantic¹¹

Boxes

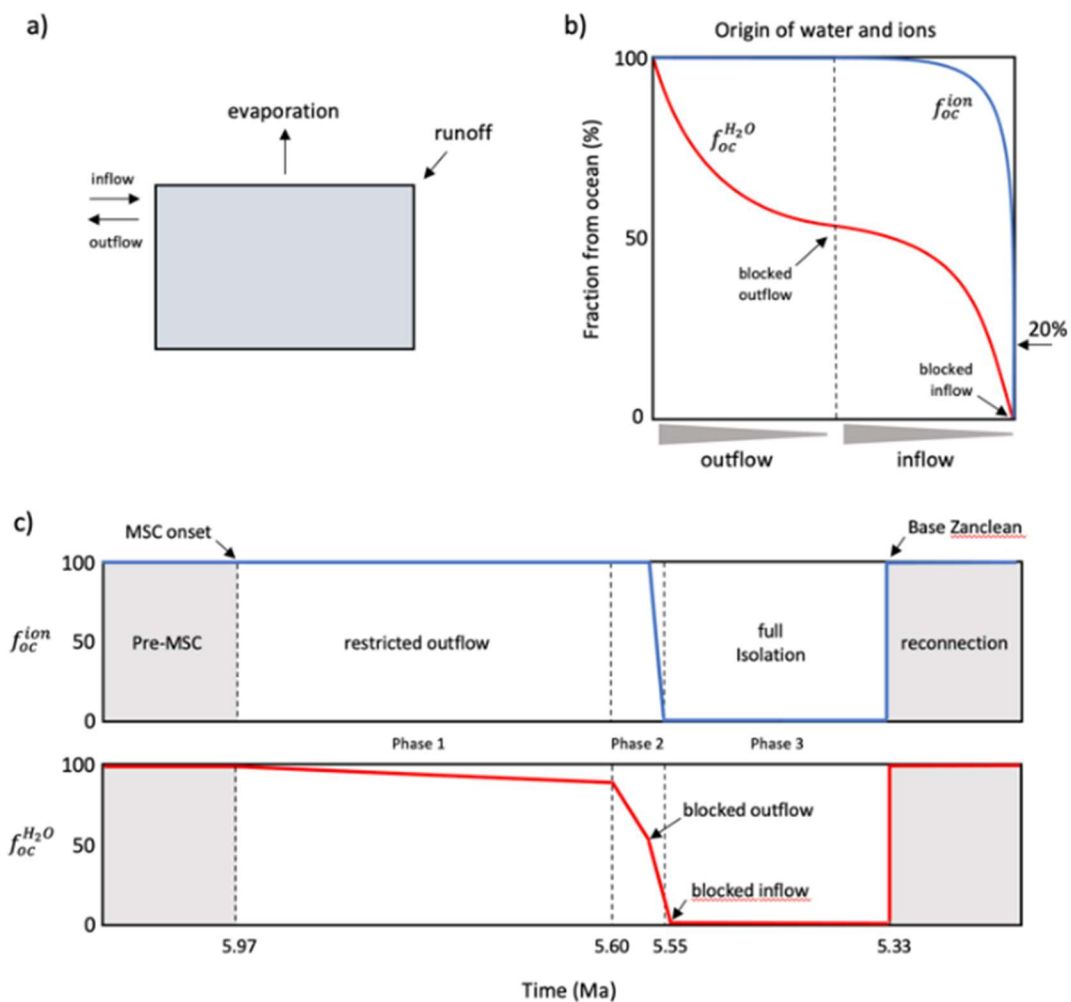
[B1] Evaporitic salt formation

Ocean chemistry has changed substantially over time¹⁶⁹. One driver for this change is the precipitation and weathering of giant evaporite deposits. The most common marine evaporite minerals – carbonates, gypsum, anhydrite, halite, and the bittern salts (kainite, carnallite, bischofite) – precipitate from seawater when the concentration of their constituent ions (Na^+ , Cl^- , Ca^{2+} , SO_4^{2-} , K^+ , Mg^{2+} , HCO_3^-) exceeds a threshold known as the solubility product^{170,171}. Ion concentration in evaporite basins depends both on water fluxes to, and the total water volume of, the marginal basin. Ions are added to these basins by water inflow from the ocean and rivers, and leave the basins only by outflow to the ocean or by mineral precipitation. The water volume in an evaporite basin is conserved if a sufficient oceanic connection exists, but it can decline through net evaporative draw-down if the connection becomes severely restricted or blocked; in both cases net evaporative freshwater removal raises the dissolved ion concentration in basin waters. The main controls on evaporitic mineral precipitation are, therefore, the magnitude of the freshwater deficit and the extent of water-exchange limitation between basin and ocean (see the figure, part a).

The simplest conceptual model for evaporitic salt formation considers a seawater volume disconnected from the ocean, subject to evaporative draw-down, while receiving no further ions from either seawater or river runoff. The Mediterranean salt giant, however, did not form under these conditions because complete evaporation of a 3,000 m-thick seawater column, with an average salinity of ~35 ‰, would leave behind only about 40 m of halite, a fraction of what is preserved in the deep central basins (~ 2.5 km of halite).

The evaporite-forming ion concentration in river water is, respectively, typically 1000 (Na^+ , Cl^-), 100 (Mg^{2+} , SO_4^{2-} , K^+), and 10 (Ca^{2+}) times lower than in seawater^{172,173}. Consequently, continental runoff influences marine evaporite mineral precipitation only if oceanic input is restricted severely or cut off entirely. A qualitative picture of the impact of ocean-continental water mixing on dissolved ions, as a function of seawater-exchange

restriction, is shown in the figure. Evaporites only evolve toward a “continental” mineralogical signature when the continental input dominates the oceanic source. This is the case for the Upper Gypsum succession on Sicily where non-oceanic Sr isotope data from both gypsum and ostracods suggest minimal Atlantic contribution²⁴. The relative abundances of many other evaporite-forming ions are much higher in river water than in sea water (in brackets): $Mg^{2+}:Cl^- = 0.7$ (0.1), $SO_4^{2-}:Cl^- = 0.6$ (0.052), $Ca^{2+}:Cl^- = 1.2$ (0.019), $K^+:Cl^- = 0.05$ (0.018), and $HCO_3^-:Cl^- = 2.5$ (0.004). Thus, when oceanic connection is highly restricted or blocked, carbonate and gypsum precipitation dominate the typical halite-dominated marine association¹⁴¹.



In the figure, the controls on water and dissolved ion proportions from the ocean versus continental runoff during the MSC are shown in **part a**. Using a simplified water balance of an idealized marginal basin; **part b** is an illustration of how the fraction of water (red curve) and dissolved ions (blue curve) originating from the ocean change as a function of seawater-exchange flux, with the restriction at the sill separating the ocean from the marginal basin. In an idealized scheme for ocean water and ion fractions during the MSC (**part c**); note that continental runoff becomes a relevant ion source to the basin only when its marine connection is restricted severely, or cut off completely, from the ocean³⁶.